Available online at www.sciencedirect.com
SCIENCE DIRECT®
Journal of Electron Spectroscopy and Related Phenomena 136 (2004) 151–160
JOURNAL OF ELECTRON SPECTROSCOPY and Related Phenomena
www.elsevier.com/locate/elspec

Resonant inverse photoemission spectroscopy in soft X-ray region

Yasuhisa Tezuka [a,*], Shik Shin [b]

[a] *Faculty of Science and Technology, Hirosaki University, 3 Bunkyo-cho, Hirosaki 036-8561, Japan*
[b] *Institute for Solid State Physics, University of Tokyo, 5-1-5 Kashiwanoha, Kashiwa-shi, Chiba 277-8581, Japan*

Abstract

Resonant inverse photoemission spectroscopy (RIPES) measurements have been performed in the soft X-ray (SX) region. The energy region, which could not be accessible up to these days, includes core levels of many important elements to be investigated. They were applied to transition metals (TM), rare earth (RE) metals, and their compounds. Remarkable resonance enhancement was observed in Ce 4d → 4f resonance of some Ce compounds. This gives us complementary information with Ce 3d resonance IPES that was reported before. 2p and 3p resonance spectra were observed for the TM compounds. These resonances show rather weak enhancement compared with those of Ce compounds, although apparent resonance feature was observed. These results are well-reproduced by many-body configuration interaction on the basis of the Anderson impurity model. Though the study has just started, the results demonstrated the effectiveness of the RIPES measurements.

Keywords: Resonant inverse photoemission; Transition metal; Rare earth metal; Ti; Ni; Ce

1. Introduction

The inverse photoemission spectroscopy (IPES) has been an important technique to investigate a density of state (DOS) of unoccupied state. Combining with photoemission spectroscopy (PES), which measures a DOS of occupied state, IPES gives us complementary information about DOS of materials [1].

The IPES technique has two experimental modes; Bremsstrahlung isochromat spectroscopy (BIS) mode and tunable photon energy (TPE) mode. The former uses a band-pass filter and scans the excitation energy, while the latter uses a spectrometer with a fixed excitation energy. The BIS measurements are easier than TPE measurements, because it does not need a spectrometer and proper band-pass filter is available in the X-ray and vacuum ultraviolet (VUV) region. Thus, the X-ray BIS (XBIS) and UVBIS have been observed in early days.

The observation of IPES in the soft X-ray (SX) region, which means from several 10–1000 eV here, was still experimentally difficult, because the intensity of IPES is extremely weak. Spectroscopy in the SX region had been much behind up to recently, since interactions between photon and substances are very strong. It became possible after improvement of technology for optical devices and photon detectors like soft X-ray emission spectroscopy (SXES) [2,3].

In case of photoemission spectroscopy, resonant measurements became possible after the development of synchrotron radiation (SR) and have made remarkable achievements [4]. In 1994, Wibel and coworkers [5–7] measured resonant IPES (RIPES) near the Ce 3d-absorption edge (about 880 eV) and reported a strong resonance effect by using a crystal monochromator. However, IPES in the SX region had not been observed yet till very recently.

Recently, we succeeded in the observation of the IPES in the SX region using a spectrometer for the SXES [8]. We observed the resonant IPES of Ce and Ti compounds near the Ce 4d and Ti 3p absorption region [9–14].

In this paper, we describe the recent results of resonant IPES in the SX region. Since the reports of BIS measurements have been described in previous articles [15–18], the description of these experiments is omitted.

The measurements were performed for 3d transition metals (TM), 4f rare earth (RE) metals, and these compounds. Resonance measurements were performed at TM 2p and 3p-absorption edge, and RE 4d-absorption edge. Remarkable resonant effects were observed in these measurements.

* Corresponding author.
E-mail address: tezuka@si.hirosaki_u.ac.jp (Y. Tezuka).

0368-2048/$ – see front matter © 2004 Published by Elsevier B.V.
doi:10.1016/j.elspec.2004.02.142

Especially, the RE compounds that have localized 4f state shows strong enhancement, while TM compounds exhibit rather weak enhancement.

2. Historical background

History of PES and IPES can be traced back to the beginning of the 20th century. In 1905, Einstein found photoelectric effect [19]. In the photoelectric effect, the maximum energy of the emitted photoelectrons is proportional to the photon energy $h\nu$.

$$E_{\max} = h\nu - W,$$

where $E_{\max}$ and W mean the maximum energy of photoelectrons and the work function, respectively. An inverse relationship is hold between the short-wavelength cutoff of emitted X-rays, $h\nu_{\max}$, and incident electron energy, E_{kin} when electrons are incident to the solid surface

$$h\nu_{\max} = E_{\mathrm{kin}} + W$$

Duane and Hunt [20] determined Planck constant h from the relations. They observed X-ray emission with an energy $h\nu$ from X-ray tube as a function of acceleration voltage of electron and observed sharp rising of X-ray intensity at energy E_{kin}. That is the first observation of BIS in X-ray region. After that, Ohlin [21] observed the emission in higher resolution and found characteristic structures of sample at the threshold. Nijiboer [22] suggested the structures reflect DOS of unoccupied state.

In XBIS measurements, the apparatus for XPS are usually used [23]. The apparatus is commercially available now, which is equipped with a crystal spectrometer to monochromatize X-ray source of Al Kα (1486.6 eV) or Mg Kα, (1253.6 eV). Emitted photons are detected by means of photocathode and channel electron multiplier. Hillebrecht et al. [24] reported a high performance electron gun for XBIS, whose energy resolution is about 0.5 eV.

Application of a Geiger-Müller (GM) counter to ultraviolet band-pass detector made the BIS in ultraviolet region possible. Dose [25] observed UVBIS by means of the GM detector that has a band-pass around $h\nu = 9.7$ eV. The detector equips a CaF_2 window that works as a high-cut filter. The active gas in GM tube, which is typically I_2 gas, works as a low-cut filter at the ionization threshold. The pass width of I_2/CaF_2 detector is about 0.8 eV that decides the resolution of BIS measurements. After the development, many observations of UVBIS have been reported [16,17,26,27].

The band-pass detector was improved by many researchers [28–30]. Instead of I_2 gas, solid state photoemitter was also applied to the detector [31–33], which improved the practical resolution of UVBIS to about 0.3–0.4 eV.

In 1983, Himpsel and coworkers [34,35] observed IPES spectra in the TPE mode by means of a grating type spectrometer and position sensitive detector. They observed the IPES in the energy range $h\nu = 10$–40 eV. The TPE measurements are effective to observe a band structure in unoccupied state. Hu et al. [36] observed IPES of Sc metal at Sc 3p threshold (10–44 eV) and observed strong resonance. Since they used a near-normal-incidence spectrometer, experiments in the higher energy could not be performed.

A trial to observe IPES in the TPE mode was also made in the X-ray region. A pioneering work has been done by Liefeld and coworkers [37,38] in 1974. They observed resonant X-ray emission of La at the M_5 absorption edge. 20 years later, Wibel and coworkers [5–7] measured resonant IPES near the Ce 3d-absorption edge (about 880 eV) and reported a strong resonance effect. However, since they used a crystal spectrometer, lower limit of available energy range was about 850 eV.

Up to recently, observation of IPES in the SX region was impossible. On the other hand, the observation of SXES has become possible in the energy region from several 10 to 100 eV, recently [2,3]. SXES measurement excited by photon from synchrotron radiation was performed and achieved a lot of fruitful results.

3. Formalities

3.1. Normal IPES

IPES is generally considered as the time reversal process of photoemission. The IPES measurement observes energies of photons emitted from a sample excited by electrons, while PES measurement observes energies of electrons emitted from a sample excited by photons. Thus, the two measurements observe different properties of the sample. The IPES observes DOS of unoccupied state, while PES observes that of occupied state. Thus, the IPES and PES measurements give us complementary information of sample. Since the initial state of IPES and the final state of PES are continuous state, spectra of both measurements basically reflect the total DOS. X-ray absorption spectroscopy (XAS) and XES are also used to study the DOS, but these spectra reflect partial DOS of unoccupied and occupied states, respectively, because these are optical dipole transition. In order to elucidate the total electronic structures of a material, it is desirable to perform all these measurements. However, the IPES has been applied to only limited samples, because of its experimental difficulty.

Present situation of IPES resembles to the situation of PES around 1980, in which days resonant PES was performed in VUV region [39]. Roughly speaking, the present resolution of IPES is about 10^2 times of PES and intensity of IPES is less than 10^{-2} times of PES. The reason is due to weak intensity of IPES.

Pendry [40] estimated the intensity of IPES for the first time in analogy to the one-step model of photoemission. From the recent result of Johnson and Davenport [41], the

cross-section of IPES is described as follows

$$\frac{d\sigma}{d\Omega} = \frac{\alpha}{2\pi}\frac{\omega}{mc^2}\frac{1}{\hbar k}\left|\langle b\left|\hat{\varepsilon}\cdot p\right|k\rangle\right|^2$$

where k denotes the initial state with no photons and b denotes the final state consisting of an electron in a bound state. The $\hat{\varepsilon}$ is the polarization vector of photons, and α is the fine structure constant.

$$\alpha = \frac{e^2}{\hbar c} \approx \frac{1}{137}$$

The cross-section of PES calculated with the same assumption is described as below

$$\frac{d\sigma}{d\Omega} = \frac{\alpha}{2\pi}\frac{k}{m^2}\frac{1}{\hbar\omega}\left|\langle k\left|\hat{\varepsilon}\cdot p\right|b\rangle\right|^2$$

If we suppose the square of the matrix elements in each equation is same, the ratio of two cross-sections is given by the following equation

$$r = \left(\frac{d\sigma}{d\Omega}\right)_{\mathrm{IPES}} / \left(\frac{d\sigma}{d\Omega}\right)_{\mathrm{PES}} = \frac{\omega^2}{c^2k^2} = \left(\frac{\lambda_e}{\lambda_p}\right)^2,$$

where λ_e and λ_p are the electron and photon wavelength, respectively. The value of r is about 10^{-5} and 10^{-3} at energy of 10 eV (VUV) and 1000 eV (X-ray), respectively. This result indicates the inherent low intensity of IPES.

Fig. 1 shows the energy diagram of IPES. The IPES technique has two measurement modes; Bremsstrahlung isochromat spectroscopy mode and tunable photon energy mode. The BIS measurement observes a specific photon energy by means of a band-pass filter. The proper band-pass filter is available in X-ray (1253.6 and 1486.6 eV) and VUV (about 10 eV) region. Thus, the X-ray BIS and UVBIS have been observed in early days. The BIS spectra are recorded versus excitation energy. The BIS measurements can observe one spectrum for one sample except for angle resolved measurements, so that resonance features cannot be observed.

On the other hand, TPE measurement observes emission spectra by means of a spectrometer when the system is excited by certain energy. The TPE spectrum is plotted versus photon energy. In the TPE mode, excitation energy can be changed at will, so that the energy can coincide with the absorption edge.

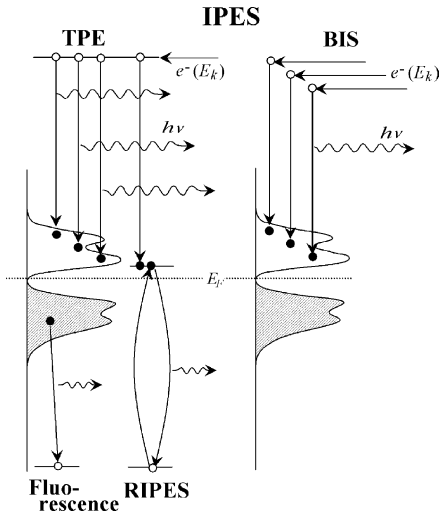

Fig. 1. Energy diagram of IPES. At low energy excitation, only IPES process is observed. If the excitation is higher than absorption edge, core hole is created. The core hole decays with fluorescence. Near absorption edge, RIPES process can take place.

3.2. Resonant IPES

In the normal IPES process, an electron incident upon a solid surface decays radiatively to the lower energy states. In the $3d^n$-electron system, for example, the normal IPES process is expressed as follows

$$\left|3d^n\right\rangle + e^- \rightarrow \left|3d^{n+1}\right\rangle + h\nu \quad (1)$$

where e^- denotes the incident electron. If the electron energy is higher than the binding energy of a core electron, the electron is excited and ejected out of the system. Then, the created core hole decays radiatively (fluorescence process) or non-radiatively (Auger process). The fluorescence process is expressed as described below

$$\left|\underline{c}3d^n\right\rangle \rightarrow \left|3d^{n-1}\right\rangle + h\nu \quad (2)$$

where $\underline{c}$ denotes a core hole. On the other hand, if the energy of the incident electron is close to the binding energy of the core hole, the second order process as described below would take place

$$\left|3d^n\right\rangle + e^- \rightarrow \left|3p^5 3d^{n+2}\right\rangle \rightarrow \left|3d^{n+1}\right\rangle + h\nu \quad (3)$$

This is a time reversal process of Auger decay. Because of the interference between processes (1) and (3), resonant effect would be observed.

In the SX region, there are many important core levels. Fig. 2 shows the energies of the core levels, compared with available energies of the several measurements modes. Almost all 2p and 3p levels of transition metals and 4d level of rare earth metals are in the SX region. 1s levels of C, N, and O are also included, as well as Si 2p. These levels have been studied with the resonant PES, and are also the subject of resonant IPES.

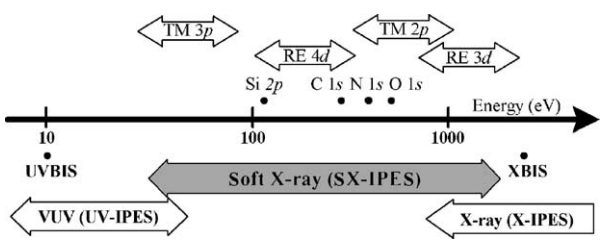

Fig. 2. Binding energies of some elements (upper) and several measurement modes (lower). TM and RE means transition metal and rare earth metal, respectively.

The fluorescence is usually observed in the emission spectra when the excitation energy is higher than absorption edge and core hole is created. The fluorescence has a unique energy of the elements in the materials to be observed. The energy is independent from the excitation energy; i.e. characteristic fluorescence. On the other hand, IPES changes its energy with changing the excitation energy. As described above, the maximum of IPES energy, which corresponds to the Fermi edge, is proportional to the excitation energy. Thus, the spectrum of the Fermi edge moves in the emission spectra by changing energy.

The relation between IPES and XES resembles that between PES and Auger electron spectroscopy (AES) spectra. The AES peak that has a unique kinetic energy is observed in a PES spectrum. When the photon energy for excitation is changed, the AES peaks move in the PES spectrum. The resonance effect is observed, when an AES peak coincides with a certain PES peak; i.e. these processes have the same initial and final states. Similarly, the resonance effect is observed in IPES when the fluorescence peak matches with a certain IPES peak.

4. Experiments

4.1. Overview

Fig. 3 shows the schematic diagram of a spectrometer of IPES. The apparatus was originally developed for XES [8]. The XES measurements were performed using synchrotron radiation in place of the electron gun in the figure.

In case of resonant IPES, the intensity is enhanced strongly. Especially, strongly correlated materials such as Ce compounds show strong enhancement when Ce 3d core level matches with the photon energy [5]. The intensity of an on-resonant spectrum becomes over 10^2 times of an off-resonant spectrum. However, Ce 4d resonance does not show such a strong enhancement and TM 2p and 3p resonance shows rather weak resonance. Thus, the observation of RIPES in the SX region is rather difficult compared with the Ce 3d systems.

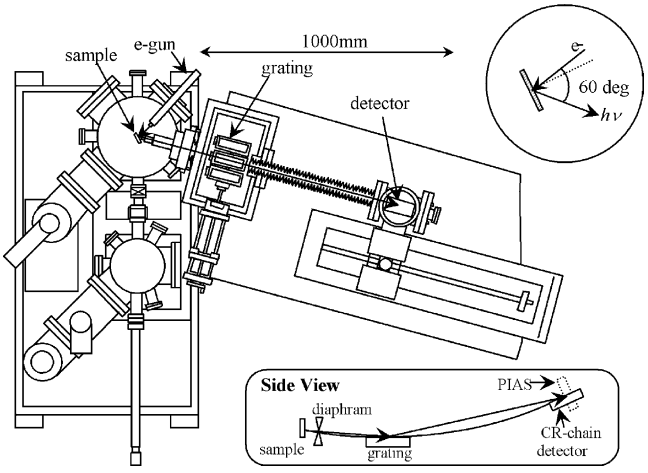

Fig. 3. Schematic diagram of spectrometer for IPES. The angle between incident electron and emitted photon is 60°. The inset shows the side view. A Rowland-mount type spherical-grating spectrometer is used.

Pressure of the main chamber should be kept under 1×10^{-10} Torr, because the IPES is very sensitive to surface state and the measurements time is usually long.

4.2. Spectrometer

The spectroscopy in the VUV and X-ray region has been a challenging subject, because of its experimental difficulties. However, thanks to the advent of synchrotron radiation, the spectroscopic technology has rapidly improved. A number of types of grazing-incidence spectrometers were developed and simultaneously, X-ray emission measurements became possible in the soft X-ray region [2,3].

Rowland mount type spectrometer is used in this study. Two types of spherical gratings, 5 m with 300 lines per millimeter and 7 m with 1200 lines per millimeter, were used. The incidence angle of the spectrometer was fixed at an angle of 85.98 and 87.13°, respectively. The spectrometer covers the energy range from 30 to 1200 eV. Detection angle of the spectrometer is about 1∼2 srad. The designed resolution is 0.04 and 0.15 eV at the energy of 50 and 100 eV, respectively, when 5 m grating is used, and 1.0 eV at the energy of 500 eV, when 7 m grating is used.

4.3. Electron gun

In the UVBIS measurements, the energy of electron beam is rather low (5–15 eV), so that the space charge effect cannot be disregarded. Furthermore, low angular spread and reasonably high current (∼10 μA) are required. Thus, a Pierce type electron gun [34] and pervatron [42] was used for excitation.

Since the electron energy is rather high in this study, the space charge effect is not so serious. But, small spot size of the electron beam is rather essential in this system, since the spectrometer has a small diaphragm (slit) in order to achieve high resolution. The size of effective observation spot is determined by the slit size, that is typically 50–100 μm.

At the initial stage of this study, a filament-cathode-type electron gun was used for excitation. The energy range of the gun was up to 5 keV and the spot size was comparable to the slit size, but the energy spread was rather wide. To improve the resolution, a Pierce type electron gun with BaO cathode is used. The spot size is rather large, but the energy spread is narrower than that of the filament type.

The electron kinetic energy for excitation was calibrated by energy analyzer. In the standard measurements, electrons are injected normally and the emitting photons are observed at an angle of about 60°.

The resolution of the system is limited by the energy spread of the electron gun in the low energy region. Since

the energy spread of the thermionic cathode is over than 0.2–0.3 eV even at low temperatures, the resolution of the IPES system cannot be improved beyond that energy spread.

4.4. Detector

Since the IPES intensity is extremely weak and efficiency of spectrometer is very low, high sensitive and high efficiency detector is required for SX–IPES measurements.

A position sensitive detector, which consists of microchannel plates and a resistive anode, was used for TPE measurements from the beginning of IPES measurements [34–36]. In early days, the detector was small (1 in. diameter) and has rather few channels (less than 100) to detect, but it has been improved.

In our experiments, two types of the detectors were used. One-dimensional (CR-chain, Hamamatsu Photonics) and two-dimensional (PIAS, Hamamatsu Photonics) multi-channel detectors were properly selected depending of situation.

The CR-chain with a $30 \times 80\,mm^2$ size and 1024 channels is mounted tangentially along the Rowland circle of the spectrometer. Since its detection plane is flat, the plane does not coincide completely with the Rowland circle. Furthermore, the detector has a large size ($30 \times 80\,mm^2$), so that the resolution at the edge of the detector becomes worse compared with the center.

The effective spectral range depends on both dispersion of the spectrometer and dimension of the detector. Thus, it changes by changing the energy. The effective energy range of the CR-chain is rather narrow because of the grazing-incidence setup; 15–40 eV at the detection energy of 50–120 eV (5 m grating), 160 eV at 420 eV (7 m grating). The CR-chain is suitable for measuring a narrow range in detail.

Because of the experimental arrangement, the PIAS can be used only at normal incidence. Thus, the detection plane is not always on the Rowland circle and distortion of spectral image is large. However, since the PIAS is a two-dimensional detector, correction of the distortion is easy. On the other hand, the effective spectral range becomes rather wider from 25 to 70 eV by changing the center energy from 50 to 120 eV. The PIAS is suitable for measuring the wide energy range.

Recently, flat field type spectrometer has been applied to IPES and SXES measurements [43,44]. Since the spectrometer has approximately a flat focus line, higher resolution is expected.

The absolute energies of the spectra were calibrated by measuring the Fermi edge of Au. Efficiency of detector is also calibrated by detecting white light, since the efficiency depends on the position in the detector.

Since the cross-section of emission spectra is proportional to the third power of its energy, observed spectra are normalized by $(h\nu)^3$ [45]. Furthermore, the spectra were also normalized by the emission current of electron gun.

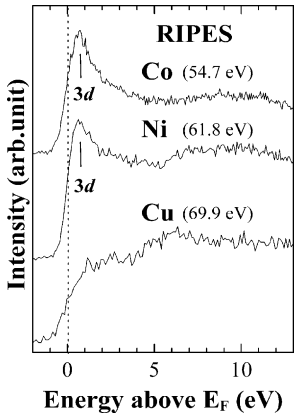

Fig. 4. IPES spectra from Co, Ni, and Cu metals. The spectra were excited by the energy below the absorption edge, so that these show DOS of these metals. Each peak just above E_F of Co and Ni is 3d peak. The 3d peak is not observed for Cu.

5. Results and discussions

5.1. 3d Transition metals and these compounds

Transition metals and these compounds are interesting materials for resonant IPES experiments. Only one result of resonance measurement has been reported for Sc 3p resonance by Hu et al. [36] using a normal incidence spectrometer.

TM 3p (40 – 70 eV) and TM 2p (400 – 900 eV) can be excited in this system. The efficiency of the spectrometer becomes lower at lower energy and the emission current of the electron gun also becomes lower. Thus, the measurement in the low energy is rather difficult.

Fig. 4 shows IPES spectra of Co, Ni, and Cu metals. These samples were prepared by evaporation on a Mo substrate. Co, Ni, and Cu metals have $3d^8$, $3d^9$, and $3d^{10}$ nominal states, that is, two, one, and no d-hole(s) in the ground state, respectively. The IPES spectra were excited at the energy below the absorption edge of each metal. Thus, these are normal IPES spectra that reflect the DOS of empty state. A sharp structure just above E_F observed in Co and Ni corresponds to 3d state, while the corresponding structure is not observed in Cu that has no 3d hole nominally.

Fig. 5 shows emission spectra of Ni, which were excited by various energies near the Ni 3p-absorption edge [46]. The observed spectra are shown with dots and the smoothed data are shown by solid lines. A few spectra at low energy excitation are normal IPES spectra. When the excitation energy is higher than 66.1 eV, core electron is excited. Then, each emission spectrum includes both IPES and fluorescence components. The fluorescence spectrum is originated from a decay of a Ni 3p core hole that is created by the incident electron. The fluorescence peak is observed at about 65 eV in these spectra. An IPES peak moves with the excitation energy. A sharp edge in each spectrum corresponds to the Fermi edge. The peak beside the Fermi edge becomes very

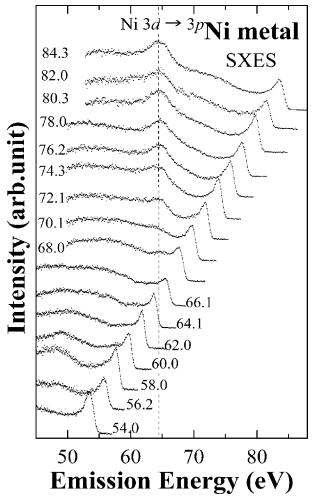

Fig. 5. SXES spectra of Ni metal. The numbers beside these spectra denote the excitation energies. The dots show observed spectrum and solid lines show smoothed data. The energy position of Ni 3d → 3p fluorescence is shown by broken line.

weak when the excitation energy is 66.1 eV, where the fluorescence peak has almost the same energy as the IPES peak.

Fig. 6 shows the RIPES spectra of Ni. On- and off-resonance spectra are plotted versus energy from E_F. An arrow shows the energy position of Ni 3d → 3p fluorescence. Ni 3d peak just above E_F becomes weak in the on-resonance spectrum.

Tanaka and Jo [47] calculated RIPES spectra of Ni by impurity Anderson model including many-body configuration interaction effect. Fig. 7 shows the calculated IPES spectra. In the calculation, the initial state of Ni metal consists of $3d^8$, $3d^9$, and $3d^{10}$ configurations, and the IPES spectrum splits to bonding, anti-bonding and non-bonding states. The bonding state becomes the main peak near the Fermi edge and it shows a Fano-type resonance [48], while non-bonding and anti-bonding peaks at 2 and 4 eV are resonantly enhanced at the absorption edge. The calculated intensity changes are

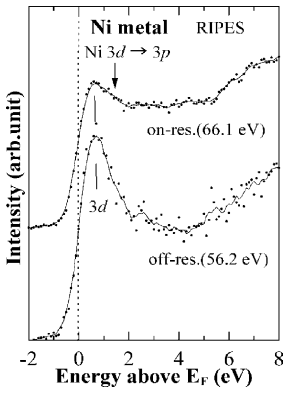

Fig. 6. RIPES spectra of Ni metal. On- and off-resonance spectra are plotted vs. energy from E_F. An arrow shows the energy position of Ni 3d → 3p fluorescence. Ni 3d peak just above E_F becomes weak in the on-resonance spectrum.

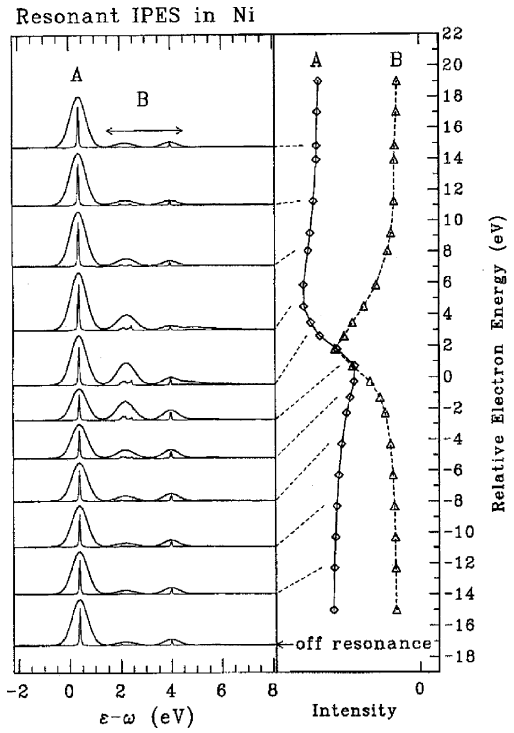

Fig. 7. Calculated IPES spectrum of Ni as a function of $E = \varepsilon - \omega$ for various ε. The ϵ dependence of the intensity of the main peak ($E \sim 0$ eV) and the shoulder ($E = 2$–4 eV) are shown by the solid and dotted lines, respectively, on the right; ε and ω denote the energies of incident electrons and emitted photons, respectively [47].

also shown in Fig. 7. These results seem to describe well qualitatively the intensity change of the spectra.

Fig. 8 shows Ti 3p RIPES spectra of lightly doped $SrTiO_3$ [14]. The resonance enhancement of the RIPES is observed at the Ti 3p → 3d-absorption edge. The figure shows on- and off-resonance spectra which are excited by 47 and 45 eV, respectively. The spectra show two features, which correspond to the t_{2g} and e_g states. In the figure, difference spectrum between these two spectra and O 1s XAS spectrum are also shown. The figure shows that the Ti 3d state is enhanced by the resonance, while the intensity of Sr 4d state is not changed. The peak at 6.1 eV is a surface state, which is expected from recent band calculation of doped $SrTiO_3$ [49].

Fig. 9 shows Ti 2p RIPES spectra of TiO_2 (rutile) plotted versus emission energy. A single-crystal was cleaned by scraping with a diamond file. SXES spectrum that is excited by SR is shown at the bottom of the figure [50]. Ti 3d → 2p emission peaks are observed in these spectra, which are shown by vertical bars in the figure. It reflects the existence of 3d electrons in the ground state, though TiO_2 is thought to be $3d^0$ system nominally.

Fig. 10 shows the RIPES spectra of TiO_2 plotted versus energy from E_F. Just above the Fermi edge, IPES spectra of Ti 3d state are observed. It can be seen that the Ti 3d peak is enhanced at the 467 eV excitation. Above that excitation energy, the IPES spectra become weak and shift its peak position. We have reported X-BIS [51] and XAS [50] result

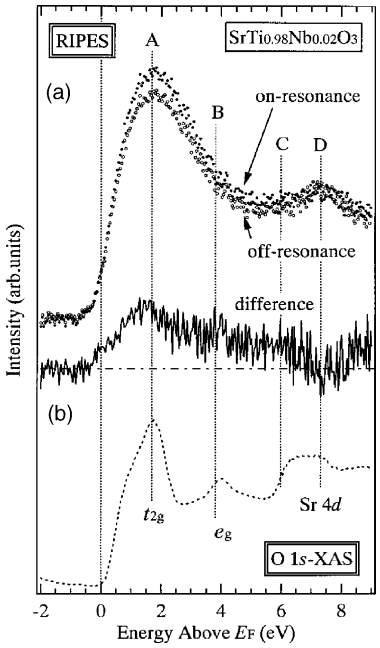

Fig. 8. RIPES spectra of $SrTi_{0.98}Nb_{0.02}O_3$ [14]. (a) On-resonance (closed circle) and off-resonance (open circle) spectra measured at $E_{ex} = 547$ and 45 eV, respectively. (b) Difference spectrum (solid line) subtracted from on- and off-resonance spectrum is also shown. (c) O 1s XAS spectrum.

of TiO_2. In the X-BIS spectrum, t_{2g} and e.g. peaks, which are caused by crystal field splitting, are observed at about 1 and 4 eV, respectively. The peak shift in the RIPES spectra might reflect these states.

5.2. 4f Rare earth metals and these compounds

Rare earth metals and these compounds are other interesting subjects of resonant IPES measurements in the SX region. Main target in this study is RE 4d core level.

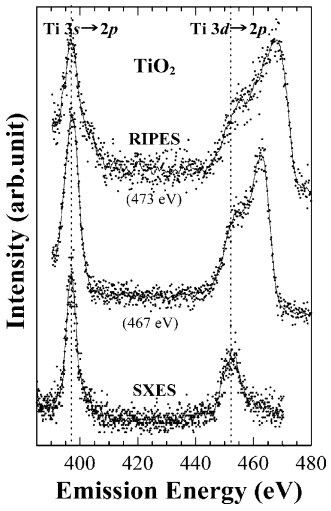

Fig. 9. Ti 2p RIPES spectra of TiO_2. The spectrum at the bottom is SXES spectrum that is excited by SR. Dotted lines denote Ti 3s → 2p and Ti 3d → 2p fluorescence. Arrows show IPES peak of Ti 3d.

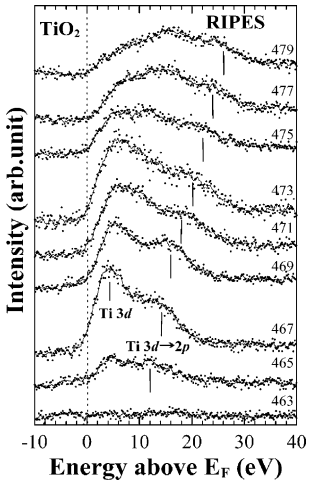

Fig. 10. RIPES spectra of TiO_2 (rutile). Numbers beside the spectra denote excitation energy. Vertical bars correspond to emission peaks: Ti 3d → 2p emission. The IPES peak of 3d just above E_F shows resonant enhancement in the spectrum.

The first observation of RIPES on the La M_5 absorption edge was performed by Liefeld and coworkers [37,38] in 1974. Several years ago, Wibel et al. [5] applied RIPES spectroscopy to the investigation of the strongly correlated electron systems. They performed RIPES measurements on the Ce M_5 edge of several 'Ce-based Kondo materials'. They observed the strong resonance effect of the Ce 4f-IPES spectra at the Ce 3d-absorption edge. Tanaka and Jo [52,53] calculated the IPES spectra within the impurity Anderson model, which includes the full multiplet coupling effects and configuration dependent hybridization strength between the 4f and conduction electrons. Their calculation explains well the resonance behaviors of observed RIPES spectra. On the other hand, the comparison between the experimental and calculated results of the RIPES spectra at the Ce $N_{4,5}$ edge of several Ce compounds was reported by Kanai et al. [13] Clear resonant spectra were observed at the $N_{4,5}$ edge because of well separated incoherent components, i.e. the normal fluorescence from the RIPES spectra.

Fig. 11 shows a comparison between RIPES spectra of two Ce compounds. A single-crystal sample was cleaned by scraping with a diamond file. The $CeGa_2$ is a dense Kondo type material, while the $CePd_7$ shows valence fluctuation. A peak at about 40 eV in each spectrum is an emission peak of Ce 5p → 4d. The peaks at Fermi edge correspond to RIPES peak of 4f empty state. Since it is observed on resonance condition, the 4f peaks are observed strongly. The RIPES spectra show contrast feature. $CePd_7$ shows two 4f peaks, while $CeGa_2$ shows only one peak. The label f^1 and f^2 in Fig. 10 denote the number of 4f electrons in the final state. On the other hand, since Ce ion in the $CeGa_2$ has just one 4f electron, the IPES shows only one peak.

Fig. 12 shows RIPES spectra of $CeGa_2$. Two series of vertical bars indicate fluorescence spectra. The f^2 peak is enhanced resonantly in the spectrum excited by 120 eV. It can

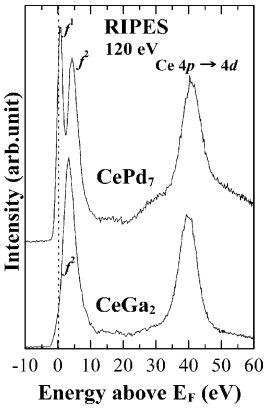

Fig. 11. Comparison of on-resonance IPES spectra between two Ce compounds, which have different electronic state in the ground state. Vertical bars indicate the peak of Ce 5p → 4d emission. The f^1 and f^2 denote the final state of RIPES process.

be seen that the Ce 4f → 4d emission peak is overlapping to the 4f peak, in which energy the 4f peak is enhanced by resonance.

Fig. 13 shows RIPES spectra of $CeRh_3$, $CePd_3$, and $CeSn_3$ [10]. The off-resonant spectra (E_{ex} = 90 eV) are shown in Fig. 13(a). The strong peak at 1.1 eV above E_F in the spectrum of $CeRh_3$ is the 'f^1 peak', which corresponds to the $4f^1$ final state. The f^1 peak contains the Kondo resonance.

The f^1 peaks of $CePd_3$ and $CeSn_3$ in Fig. 13(a) are at 0.5 eV. The T_Ks of $CePd_3$ and $CeSn_3$ are around 200 K. The f^1 peak of $CeRh_3$ is much larger and it is situated at the higher energy side as compared with those of $CePd_3$ and $CeSn_3$. This indicates the extremely higher T_K and strong

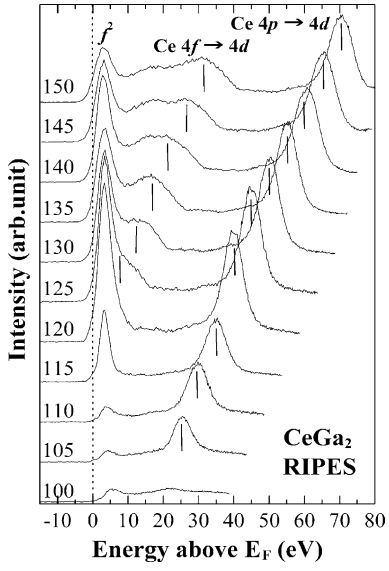

Fig. 12. Ce 4d RIPES spectra of $CeGa_2$. Numbers beside the spectra denote excitation energy. Two series of vertical bars correspond to emission peaks: Ce 4f → 4d and Ce 5p → 4d emission. The IPES peak of $4f^1 \rightarrow 4f^2$ just above E_F shows resonant enhancement in the spectrum by excitation of 120 eV.

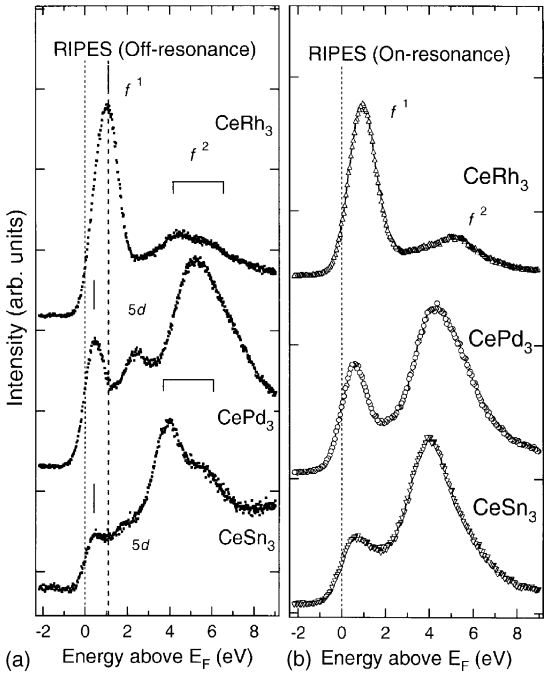

Fig. 13. (a) The off-resonant RIPES spectra of $CeRh_3$, $CePd_3$, and $CeSn_3$. The abscissa is the energy above Fermi level (E_F). The measurements were performed at 25 K. (b) The on-resonant RIPES spectra of $CeRh_3$, $CePd_3$, and $CeSn_3$ [10].

itinerant character of the 4f electron of $CeRh_3$ than that of the typical valence-fluctuating systems [54].

The structures corresponding to the final state with $4f^2\underline{c}$ configuration are observed around 5 eV in the spectra of $CeRh_3$ and $CePd_3$ and 4 eV in $CeSn_3$. The f^2 peaks are found to have strong multiplet splitting which causes complicated lineshapes, as clearly shown in $CeRh_3$ and $CeSn_3$ spectra. On the other hand, the structures at 2 eV in the spectra of $CePd_3$ and $CeSn_3$ are assigned to the Ce 5d band.

Fig. 13(b) shows the on-resonant RIPES spectra. The Ce 5d band is not found in the spectra of $CePd_3$ and $CeSn_3$ due to the resonance enhancement of 4f components. Reduction of spectral intensity at E_F in the on-resonant spectrum of $CeRh_3$ is caused by the lack of the 5d band contribution just above E_F. Thus, the on-resonance spectra in Fig. 13(b) can be regarded as the $4f^1$ contribution itself.

The f^1 peak intensity of $CeRh_3$ is extremely large as compared with those of $CePd_3$ and $CeSn_3$. Furthermore, the intensity at E_F is small. This directly reflects the highest T_K and that the $4f^0$ configuration is dominant in the initial state. This is consistent with the extremely low value of Pauli-like susceptibility χ_0 of $CeRh_3$ [55,56]. The remarkable itinerant character of 4f electrons of $CeRh_3$ is reflected by the strongly depressed f^2 peak. The $CeRh_3$ can be regarded as the most α-like Ce compound. Similar remarkable properties are reported for $CePd_7$ [9].

The f^1 peak of $CeSn_3$, which is not seen clearly in the off-resonant spectrum in Fig. 13(a), appears in the

on-resonant one in Fig. 13(b), distinctly. The T_K of $CePd_3$ has been reported to be about 240 K and that of $CeSn_3$ to be about 200 K [57,58]. They have very similar Kondo temperature. It is interesting that the relative f^1 peak of $CeSn_3$ is much smaller than that of $CePd_3$ irrespective of similar T_K. This directly indicates the fact that there is a big difference in the initial state configurations, i.e. in the 4f occupancy nf, between $CePd_3$ and $CeSn_3$ [13].

6. Summary

Resonant inverse photoemission studies were performed for transition metals, rare earth metals and these compounds. Remarkable resonance was observed in these materials. Ce 4d → 4f resonance of some Ce compounds shows drastic enhancement.

The resonant IPES measurements have just started. This gives useful information of the electronic structures complementary to resonant PES. A number of applications can be considered in the SX region. However, the present IPES technique has still problems that should be solved. Most important issue is the improvement of energy resolution, which is about 0.5 eV at present, the same level as that of PES in 20 years ago. Angle resolved and spin resolved studies have bee realized in UVBIS [18,59], and quite popular in PES, but not in IPES. Such experiments in IPES are also necessary to be developed in the SX region.

Acknowledgements

Authors thank to Dr. Tanaka and Prof. Jo for their useful discussions, and to Prof. A. Kakizaki and T. Sato for sample offering. Authors also thanks to colleagues Dr. K. Kanai, Dr. T. Higuchi, Dr. H. Ishii, and Dr. S. Nozawa.

References

[1] J.B. Pendry, Phys. Rev. Lett. 45 (1980) 1356.
[2] J. Nordgren, G. Bray, S. Cramm, R. Nyholm, J.-E. Rubensson, N. Wassdahl, Rev. Sci. Instrum. 60 (1989) 1690.
[3] T.A. Callcott, K.L. Tsang, C.H. Zhang, D.L. Ederer, E.T. Arakawa, Rev. Sci. Instrum. 57 (1986) 2680;
D. L. Ederer, J. H. McGuire, Raman Emission by X-ray Scattering, World Scientific, Singapore, 1996.
[4] L.C. Davis, J. Appl. Phys. 59 (1986) R25.
[5] P. Weibel, M. Grioni, D. Malterre, B. Dardel, Y. Bear, Phys. Rev. Lett. 72 (1994) 1252.
[6] P. Weibel, M. Grioni, C. Hêche, Y. Baer, Rev. Sci. Instrum. 66 (1995) 3755.
[7] M. Grioni, P. Weibel, D. Malterre, Y. Bear, D. Duo, Phys. Rev. B55 (1997) 2056.
[8] S. Shin, A. Agui, M. Fujisawa, Y. Tezuka, T. Ishii, N. Hirai: Rev. Sci. Instrum. 66 (1995) 1584.
[9] K. Kanai, Y. Tezuka, M. Fujisawa, Y. Harada, S. Shin, G. Schmerber, J.P. Kappler, J. Parlebas, A. Kotani, Phys. Rev. B55 (1997) 2623.
[10] K.S. Shin, J. Electron Spectrosc. Relat. Phenom. 92 (1998) 77.
[11] T. Higuchi, T. Tsukamoto, M. Tanaka, H. Ishii, K. Kanai, Y. Tezuka, S. Shin, H. Takei, J. Electron Spectrosc. Relat. Phenom. 92 (1998) 71.
[12] K. Kanai, T. Terashima, Y. Muro, M. Ishikawa, T. Uozumi, A. Kotani, G. Schmerber, J.P. Kappler, J. Parlebas, S. Shin, Phys. Rev. B 60 (1999) 5244.
[13] K. Kanai, Y. Tezuka, T. Terashima, A. Kotani, T. Uozumi, G. Schmerber, J.P. Kappler, J. Parlebas, S. Shin, Phys. Rev. B. 63 (2001) 033106.
[14] T. Higuchi, S. Nozawa, T. Tsukamoto, H. Ishii, R. Eguchi, Y. Tezuka, S. Yamaguchi, K. Kanai, S. Shin, Phys. Rev. B. 66 (2002) 153105.
[15] V. Dose, J. Phys. Chem. 88 (1984) 1681.
[16] F.J. Himpsel, Th. Fauster, J. Vac. Sci. Tech. A. 2 (1984) 815.
[17] D.P. Woodruff, P.D. Johnson, N.V. Smith, J. Vac. Sci. Tech. A. 1 (1983) 1104.
[18] N.V. Smith, Rep. Prog. Phys. 51 (1988) 1227.
[19] A. Einstein, Ann. Phys. Lpz. 17 (1905) 132.
[20] W. Duane, F.L. Hunt, Phys. Rev. 6 (1915) 166.
[21] P. Ohlin, Ark. Mat. Astro. Fys. A 29 (1942) 3.
[22] B.R. Nijiboer, Physica 12 (1946) 461.
[23] J.K. Lang, Y. Baer, Rev. Sci. Instrum. 50 (1979) 221.
[24] F. Hillebrecht, et al., Rev. Sci. Instrum. 58 (1987) 776.
[25] V. Dose, Appl. Phys. 14 (1977) 117.
[26] V. Dose, Prog, Surf. Sci. 13 (1983) 225.
[27] V. Dose, J. Phys. C 14 (1984) 1681.
[28] V. Dose, Th. Fauster, R. Schneider, Appl. Phys. A 40 (1986) 203.
[29] P.M.G. Allen, P.J. Dobson, R.G. Egdell, Solid State Commun. 55 (1985) 701.
[30] D. Funnemann, H. Merz, J. Phys. E: Sci. Instrum. 19 (1986) 554.
[31] N. Babbe, W. Drube, M. Schäfer, M. Skibowski, J. Phys. E. Sci. Instrum. 18 (1985) 158;
I. Schäfer, W. Drube, M. Schlüter, G. Plagemann, M. Skibowski, Rev. Sci. Instrum. 58 (1987) 710.
[32] Y. Ueda, K. Nishihara, K. Mimura, Y. Hari, M. Taniguchi, M. Fujisawa, Nucl. Instrum. Methods A 330 (1993) 140.
[33] F. Schedin, G. Thornton, R.I.G. Uhrberg, Rev. Sci. Instrum. 68 (1997) 41.
[34] Th. Fauster, F.J. Himpsel, J.J. Donelon, A. Marx, Rev. Sci. Instrum. 54 (1983) 68.
[35] Th. Fauster, D. Straub, .J.J. Donelon, D. Grimm, A. Marx, F.J. Himpsel, Rev. Sci. Instrum. 56 (1985) 1212.
[36] Y. Hu, T.J. Wagener, Y. Gao, J.H. Weaver, Phys. Rev. B. 38 (1988) 12708.
[37] R. Liefelt, A.F. Burr, M.B. Chamberlain, Phys. Rev. A. 9 (1974) 316.
[38] M.B. Chamberlain, A.F. Burr, R. Liefelt, Phys. Rev. A 9 (1974) 663.
[39] C. Guillot, Y. Ballu, J. Paigné, L. Lecante, K.P. Jain, P. Thiry, R. Pinchaux, Y. Pétroff, L.M. Falicov, Phys. Rev. Lett. 39 (1977) 1632.
[40] J. Pendry, Phys. Rev. Lett. 45 (1980) 1356.
[41] P.D. Johnson, J.W. Davenport, Phys. Rev. B 31 (1985) 7521.
[42] N.G. Stoffel, P.D. Johnson, Nucl. Instrum. Methods A 234 (1984) 230.
[43] H. Sato, T. Kotsugi, S. Senba, H. Namatame, M. Taniguchi, J. Synchrotron Radiat. 5 (1998) 772.
[44] T. Tokushima, Y. Harada, M. Watanabe, Y. Takata, E. Ishiguro, A. Hiraya, S. Shin, Surf. Rev. Lett. 9 (2002) 503.
[45] The Quantum Theory of Radiation, W. Heitler (Ed.), Oxford University Press, Oxford, 1944.
[46] Y. Tezuka, K. Kanai. H. Ishii, S. Shin, A. Tanaka, T. Jo, in preparation.
[47] A. Tanaka, T. Jo, J. Phys. Soc. Jpn. 66 (1997) 1591.
[48] U. Fano, Phys. Rev. 124 (1961) 1866.
[49] D. Sarma, S.R. Barman, H. Kajueter, G. Kotliar, Europhys. Lett. 36 (1996) 307.
[50] Y. Tezuka, S. Shin, A. Agui, M. Fujisawa, T. Ishii, J. Soc. Phys. Jpn. 65 (1996) 312.
[51] Y. Tezuka, S. Shin, T. Ishii, T. Ejima, S. Suzuki, S. Sato, J. Phys. Soc. Jpn. 63 (1994) 347.

[52] A. Tanaka, T. Jo, Physica B 206/207 (1995) 74.
[53] A. Tanaka, T. Jo, J. Phys. Soc. Jpn. 65 (1996) 615.
[54] J.G. Sereni, O. Trovarelli, A. Herr, J.Ph. Schillé, E. Beaurepaire, J.P. Kappler, J. Phys.: Condens. Matter 5 (1993) 2927.
[55] J.P. Kappler, P. Lehman, G. Shmerber, G.L. Nieva, J.G. Sereni, J. Phys. Paris 49 (1988) C8–721.
[56] J.P. Kappler, G. Shmerber, J.G. Sereni, J. Magn. Magn. Mater. 79–77 (1988) 185.
[57] M.J. Besnus, J.P. Kappler, J. Phys. F 13 (1983) 157.
[58] J.G. Sereni, J. Less-Common Met. 84 (1982) 1.
[59] J. Kirschner, M. Glöbl, V. Dose, H. Scheidt, Phys. Rev. Lett. 53 (1984) 612.